3D velocity-independent elliptically-anisotropic moveout correction[a]

[a]Published in Geophysics, 74, no. 5, WB129-WB136, (2009)

William Burnett and Sergey Fomel

ABSTRACT

Azimuthal anisotropy or lateral velocity variations cause azimuthal variations in moveout velocity which can lead to seismic image degradation if not properly handled. In cases where apparent azimuthally anisotropic moveout is present, a single picked velocity is inadequate to flatten an event on a 3D CMP gather. Conventional velocity analysis techniques require a significant amount of time and effort, especially in areas where apparent anisotropy is observed. We propose a velocity-independent imaging approach to perform an elliptically anisotropic moveout correction in 3D. The velocity-independent approach relies on volumetric local traveltime slopes rather than aggregate velocities, and therefore provides an azimuthally flexible description of traveltime geometries throughout the gather. We derive theoretical expressions for extracting the moveout slowness matrix and the angle between the symmetry and acquisition axes as volumetric local attributes. A practical inversion scheme to extract the same parameters is also developed. These parameters are used to solve for moveout slowness as a function of azimuth. Tests on a synthetic CMP gather show accurate results for the automatic moveout correction and the inversion scheme. A field data example from West Texas illustrates the application of the automatic moveout correction as a residual moveout.

INTRODUCTION

Common geological occurrences such as dipping interfaces, lateral velocity variations, or HTI media can lead to real or apparent azimuthal anisotropy, in which case the P-wave moveout velocity becomes elliptically dependent on azimuth (Grechka and Tsvankin, 1998). The symmetry axes of apparent azimuthal anisotropy often correspond to geologically meaningful parameters such as the strike and dip directions of the reflector (Levin, 1985),the directions of tectonic stress (Sicking et al., 2007), the preferred orientation of vertical fractures (Crampin, 1984), or any combination of these factors. Failure to account for azimuthal velocity variations often leads to stack degradation, improper time-to-depth conversion, inaccurate AVO/AVOA, and overall poorer image results (Williams and Jenner, 2002). Sicking and Nelan (2008) and Treadgold et al. (2008) demonstrate that migration algorithms which can han-

dle azimuthal variations in the velocity model can visibly improve seismic imaging results.

Conventional manual velocity analysis procedures take up a significant part of the time needed to process seismic data. Even with semi-automated picking tools, this phase of a typical processing flow alone may take weeks or even months for modern 3D data sets. Accurate automated traveltime picking algorithms are the main tools for modern velocity analysis, and have greatly reduced the time and manual work required to hand-pick velocities (Siliqi et al., 2003). However, these tools still require significant manual inspection and editing for quality control.

The conventional production processing flow does not include picking azimuthally-dependent velocities, but two approaches are commonly used to handle and characterize azimuthal variations in velocity. The first, and historically more popular approach, is to sort CMP gathers into azimuth sectors, and then perform isotropic velocity analysis, processing, and migration on each sector. The individual moveout parameters from all sectors are plotted together, and then fit with a sinusoid to characterize the principal moveout directions and the percentage of anisotropy. Grechka et al. (1999) describe another approach, where NMO is first performed with a smooth global velocity model. If apparent anisotropy is detected, trace-to-trace traveltime shifts are estimated automatically, and the traveltime surface is fit with an ellipse characterized by the moveout slowness matrix $\mathbf{W}$. The second approach has become more popular in production because of its robustness, and in a case-study comparing the two, Lynn (2007) provides an example where the non-sectoring approach yielded a more reliable azimuthal velocity model.

The concept of velocity-independent imaging (Ottolini, 1983) is attractive because it can be very efficient when compared the time and manual work required to hand-pick velocities (Fomel, 2007). The underlying strategy of velocity-independent imaging relies on measuring traveltime slopes throughout the data set rather than hyperbolic traveltimes or velocities themselves (Wolf et al., 2004). Fomel (2002) demonstrates that plane-wave destruction filters provide an automated and effective way to measure local slopes in a seismic volume. Measured slopes can then be used to automate any common time-domain imaging step (Fomel, 2007). Previous work concerning automatic moveout corrections does not extend to the 3D case. In doing so here, we demonstrate that the azimuthal flexibility of automatic moveout correction in 3D is especially useful in the presence of real or apparent azimuthal anisotropy.

Rather than using a single picked velocity profile to apply the NMO correction, using the local slopes of a given 3D reflection event allows the event to be flattened regardless of azimuthal variations in NMO velocity. In practice, these slopes can be measured automatically throughout the volume, so no traveltime surfaces need to be picked. The velocity-independent approach can still be used to extract moveout or interval velocities throughout the data set as data attributes (Fomel, 2007). Our method also suggests that, by measuring local curvatures throughout the seismic data volume, the orientation of the symmetry axes can automatically be estimated with respect to the acquisition coordinates. We present theoretical expressions for

azimuthal anisotropy moveout parameters as volumetric attributes, and demonstrate a practical inversion scheme for the same parameters using the velocity-independent approach. Synthetic and field examples are used to validate our proposed method and show the variety of potential applications.

THEORY

Following (Grechka and Tsvankin, 1998), the elliptical NMO equation in 3D can be written with the help of a truncated Taylor series expansion as,

$$t_0 = \sqrt{t^2 - (W_x x^2 + W_y y^2 + 2W_{xy} xy)}, \tag{1}$$

where t is the event arrival time, t_0 is the moveout corrected time, and x and y are the components of full offset in the x and y survey directions, respectively. W_x and W_y are the conventionally-measured moveout slownesses squared values (along the same survey coordinates). Equation 1 describes NMO with elliptical velocity, where the third parameter, W_{xy}, arises from observing the ellipse from rotated coordinates. In practice, one can perform elliptically anisotropic NMO using conventional velocity picking in the inline and crossline directions, but the principal directions of moveout must also be estimated. Rewriting equation 1 as a matrix-vector multiplication between the offset vector and the slowness matrix $\mathbf{W}$ allows one to solve for the angle between the acquisition coordinates and the medium symmetry axes, denoted as α here. This can be done either by finding the eigenvectors of the system (Grechka and Tsvankin, 1998), or by using geometric arguments and well-known relations between the formulas for a rotated ellipse and its unrotated equivalent (Weisstein, 2009). Using the latter approach gives an expression for α in terms of conventional slowness parameters,

$$\alpha = \frac{1}{2} \tan^{-1} \left(\frac{2W_{xy}}{W_x - W_y} \right). \tag{2}$$

In this expression, α is the angle from a survey axis measured counter-clockwise toward the nearest symmetry axis. If W_x is equal to W_y, then the arc-tangent argument goes to infinity, corresponding to $\alpha = 45°$. Although equation 2 is a straightforward way of finding the coordinate rotation angle, finding the eigenvalues and eigenvectors allows one to resolve between the fast and slow principal moveout directions. The eigenvalues λ_1 and λ_2 of the slowness matrix,

$$\mathbf{W} = \begin{pmatrix} W_x & W_{xy} \\ W_{xy} & W_y \end{pmatrix}, \tag{3}$$

can be found following Grechka and Tsvankin (1998). Rewritten here in our notation, they demonstrate how the eigenvalues,

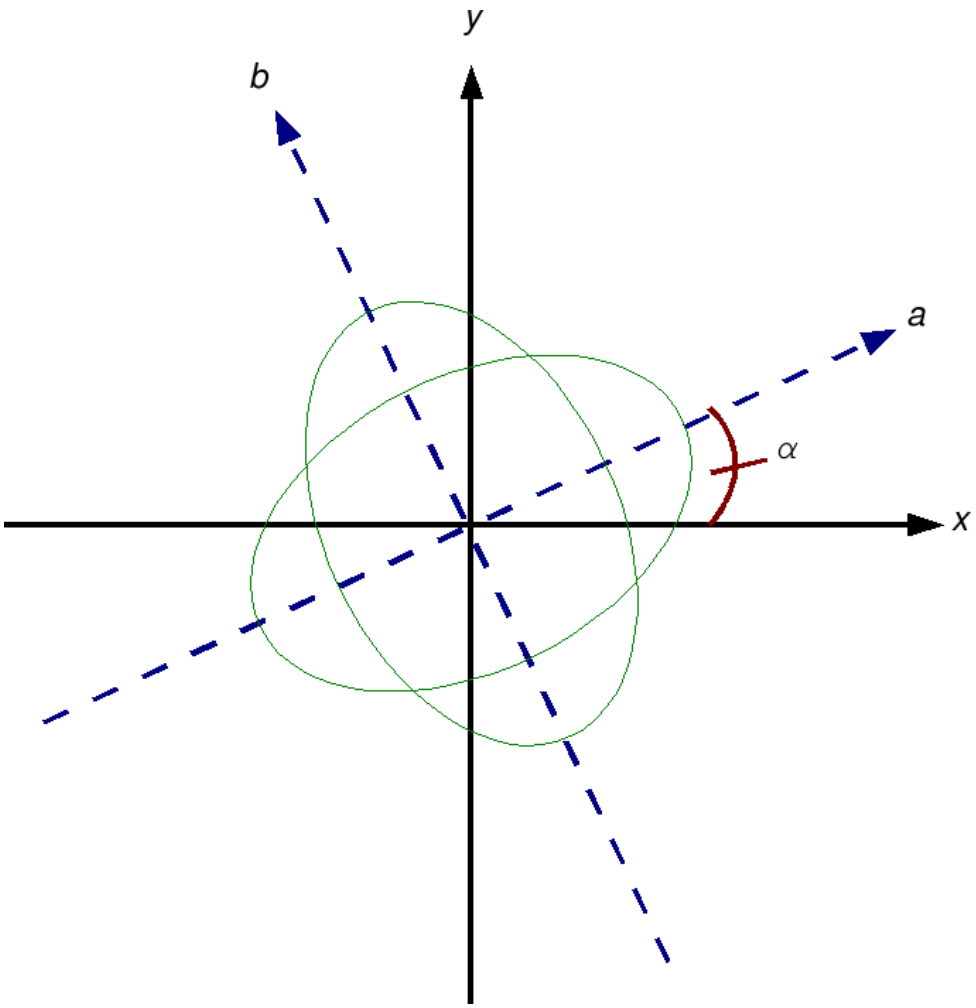

Figure 1: Elliptic NMO velocity depends on the natural symmetry axes (a-b), not the acquisition coordinates (x-y). The angle α describes the counter-clockwise rotation between the two coordinate frames.

$$\lambda_{1,2} = \frac{1}{2}\left[W_x + W_y \pm \sqrt{(W_x - W_y)^2 + 4W_{xy}^2}\right], \tag{4}$$

can be used together with α to solve for the NMO slowness S as a function of source-receiver azimuth θ:

$$S_{nmo}^2(\theta) = \lambda_1 \cos^2(\theta - \alpha) + \lambda_2 \sin^2(\theta - \alpha). \tag{5}$$

Since equation 1 describes the predicted hyperbolic traveltime curve on a CMP gather for a variety of cases where either real or apparent elliptical anisotropy may be present, the local slope of an event on an inline or crossline CMP gather can be related to the conventional moveout slowness parameters by taking the derivative of 1 with respect to x and y. Ignoring higher order terms and assuming the parameters vary slowly along x and y, gives a first-order approximation of how the measured slopes relate to conventional moveout parameters:

$$p_x(t,x,y) = \frac{\partial t}{\partial x} = \frac{W_x x + W_{xy} y}{t}, \tag{6}$$

$$p_y(t,x,y) = \frac{\partial t}{\partial y} = \frac{W_y y + W_{xy} x}{t}. \tag{7}$$

By substitution back into 1, we arrive at the velocity-independent expression for 3D elliptical moveout in terms of local slopes:

$$t_0 = \sqrt{t^2 - t\,(p_x x + p_y y)}. \tag{8}$$

Notice that only two parameters (p_x and p_y) must be measured to completely predict the NMO corrected time. More importantly, these parameters can be measured automatically using a local slope estimation algorithm, such as plane-wave destruction (Fomel, 2002). Equation 8 is a 3D extension for the 2D equation from Ottolini (1983).

Automated processes allow one to save time spent on a project, but it may seem that the insight and information gained during a more interactive conventional processing flow would be lost. A significant part of production velocity analysis involves picking or examining the velocity model directly, which provides an early and intuitive link between the seismic data and the subsurface geology. The velocity model and anisotropy information are themselves invaluable sources of geologic information. They also control the positioning of events in the final image, so an ability to extract these parameters is desirable.

The relation between local slopes and moveout velocity has been documented for the 2D case (Ottolini, 1983; Wolf et al., 2004; Fomel, 2007). In the 3D case where apparent azimuthal anisotropy is present, at least three conventional slowness

or velocity-like values are needed to characterize moveout (W_x, W_y, and W_{xy} from equation 1). Although equation 8 suggests they are not necessary for moveout in terms of local slopes, these values can be used to characterize anisotropy, and may also be useful for other subsequent processing. Simply rearranging equations 6 and 7 gives expressions for W_x and W_y:

$$W_x = \frac{tp_x - W_{xy}y}{x}, \tag{9}$$

and,

$$W_y = \frac{tp_y - W_{xy}x}{y}. \tag{10}$$

Both of these parameters require an estimate of W_{xy}. A first-order approximation of W_{xy} can be found by differentiating equation 6 with respect to y or equation 7 with respect to x:

$$W_{xy} = t\frac{\partial p_x}{\partial y} + p_x p_y = t\frac{\partial p_y}{\partial x} + p_x p_y = tp_{xy} + p_x p_y. \tag{11}$$

Since slopes are measured as a local attribute, the inline and crossline local slopes comprise data volumes with the same dimensions and coordinates as the input CMP. Applying a 1D derivative filter to these volumes allows one to obtain either mixed-derivative in equation 11, and solve for the apparent anisotropy angle α, using equation 1. This angle can also be expressed in terms of local slopes. Combining equations 9, 10, and 11 yields,

$$W_x - W_y = \frac{t}{xy}[yp_x - xp_y + (p_{xy} + (x^2 - y^2)\frac{p_x p_y}{t})]. \tag{12}$$

Now everything needed to express α independently of velocity is found in equations 11 and 12. Combining them with equation 2 gives,

$$\alpha(t,x,y) = \frac{1}{2}\tan^{-1}\left(\frac{2xy(tp_{xy} + p_x p_y)}{t(yp_x - xp_y) + (tp_{xy} + p_x p_y)(x^2 - y^2)}\right). \tag{13}$$

Implementing equation 13 creates an attribute for each input data sample describing the counter-clockwise azimuthal angle between the symmetry coordinates and the acquisition coordinates. Applying NMO to this attribute volume yields $\alpha(t_0,x,y)$, which should then theoretically be constant at each time-slice if the moveout were exactly described by equation 1.

Finding local estimates of slowness and anisotropy parameters using equations 9-13 remains at this point only an interesting theoretical idea. A more robust and

practical approach to extracting velocity and anisotropy parameters is to exploit the shear number of volumetric slope measurements made to perform the velocity-independent NMO correction. For a given CMP with dimensions $(n_x \times n_y \times n_t)$, the NMO correction applies a shift of time-squared,

$$t_\Delta(t_0, x, y) = t^2(x, y) - t_0^2(x, y), \tag{14}$$

which can be automatically computed for every output coordinate using equation (8) and stored as another volume of the same dimensions. Once NMO is applied, the time axis of the CMP gather represents t_0, so the slowness matrix $\mathbf{W}$ and α should each be constant for a given time value. Each time-slice from either the data or one of the attribute volumes can be viewed as an $(n_x \times n_y)$ matrix, which can be re-indexed into a vector of length $(n_x \times n_y)$. If the x and y indexes from the time-slice are i and j respectively, then the value from position (i, j) in the matrix is mapped to the $k = i + jn_x$ position in the vector. Using this notation, a highly overdetermined problem follows from writing equation 1 as a matrix-vector multiplication:

$$\mathbf{t}_\Delta = \mathbf{X}\mathbf{w}. \tag{15}$$

where the k^{th} element of $\mathbf{t}_\Delta$ is,

$$t_{\Delta k} = t_\Delta(t_0, x_i, y_j), \tag{16}$$

the k^{th} row of $\mathbf{X}$ is given by the vector,

$$\mathbf{x}_k = \begin{pmatrix} x_i^2 & y_j^2 & 2x_i y_j \end{pmatrix}, \tag{17}$$

and

$$\mathbf{w} = \begin{pmatrix} W_x \\ W_y \\ W_{xy} \end{pmatrix}. \tag{18}$$

Linear system 15 has $(n_x \times n_y)$ equations with only three unknowns. By solving 15 for each time-slice in the output CMP, we construct the slowness matrix $\mathbf{W}(t_0)$, and use it with equations 13, 4, and 5 to extract the coordinate rotation angle $\alpha(t_0)$ and the NMO slowness as a function of azimuth, $S(t_0, \theta)$.

EXAMPLES

We provide two examples to illustrate the performance of our approach. In the first example, we consider a simple 3D synthetic CMP gather (Figure 2a) with four events,

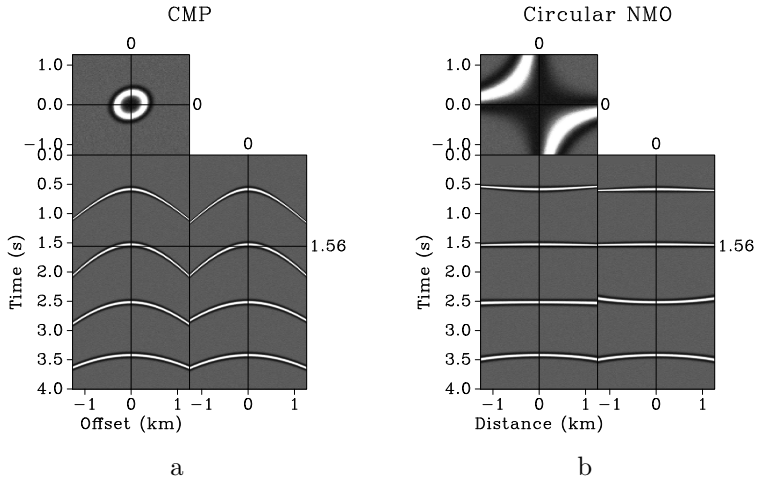

Figure 2: (a.) A synthetic 3D CMP gather with four events of varying apparent elliptical anisotropy. The three panels in the display show a time-slice view (upper square panel), a crossline view (central panel), and an inline view (right panel) of the same volume. (b.) An isotropic NMO correction using a picked velocity function appropriate for flattening certain events. At best, isotropic NMO can flatten either the inline or crossline directions well, but there is no single velocity function that will flatten both.

each with a different degree of apparent azimuthal anisotropy. The synthetic CMP in Figure 2a was created by first specifying the moveout slowness matrix, $\mathbf{W}$ for each event. Each of the four events was modeled individually by applying inverse 3D NMO to a flat reflection based on equation 1. The exact parameters used to model the four events are specified in Table 1. The four events were then added together into a single CMP gather with a small amount of random noise (10% of the signal amplitude). The result of this approach differs from real cases in that the traveltime surface for each of the events is completely independent from overlying events. However, this approach allows us to specify the exact moveout slownesses of each the events without additional work.

Event Moveout Parameters					
Event	t_0 (s)	$W_x(s^2/km^2)$	$W_y(s^2/km^2)$	$W_{xy}(s^2/km^2)$	$\alpha(^\circ)$
A	0.59	0.14	0.16	-0.01	14.0
B	1.53	0.30	0.30	-0.04	-44.3
C	2.51	0.32	0.26	-0.03	-21.8
D	3.41	0.24	0.25	-0.005	26.57

Table 1: Moveout parameters used for events in Figure 2a.

Conventional velocity semblance scans may yield multiple peaks for the same event when apparent azimuthal anisotropy is present. One must interpret the correct velocity in these areas, which can lead to inconsistent results between different processing

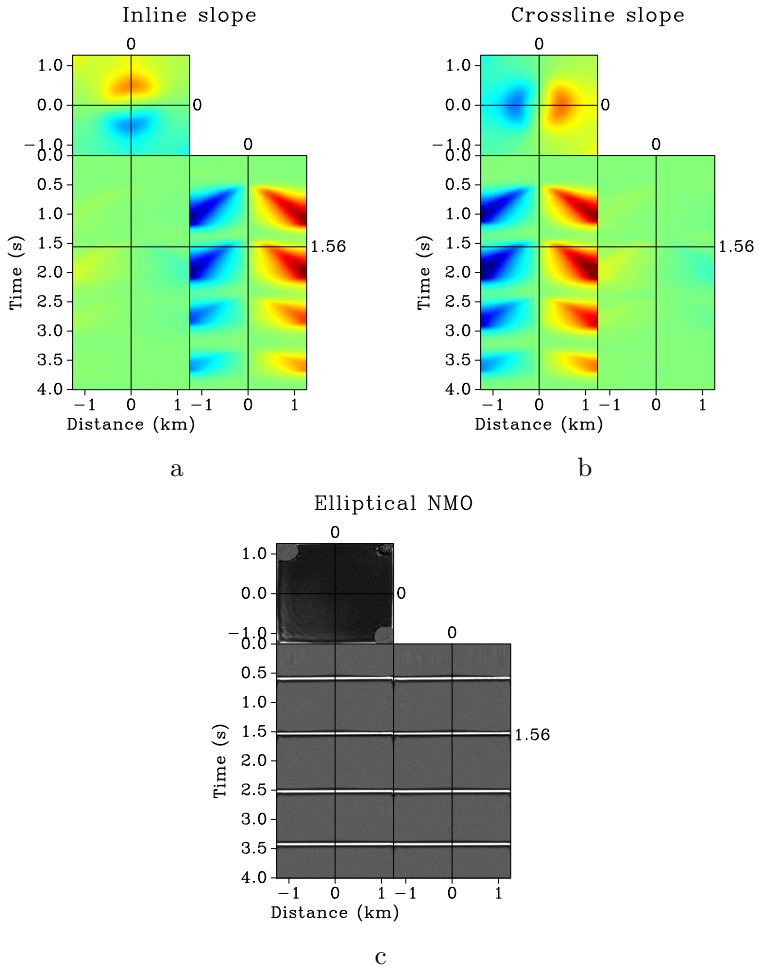

Figure 3: The (a.) inline and (b.) crossline slopes of the CMP gather from Figure 2a. (c.) These slopes are used with equation 8 to automatically perform the proposed elliptically anisotropic moveout correction. All four events are flattened perfectly where the slopes are not aliased.

geophysicists, since the cause of multiple semblance panel peaks can be ambiguous (multiples, noise, anisotropy, etc.). Resolving this ambiguity properly can add even more time and work to the production approach. Figure 2b shows a possible result of picking a single velocity profile which flattens certain events in either the inline or crossline view. For a root-mean-square velocity model, if an intermediate value is chosen for each event, both directions are flattened poorly. Event B has a particularly difficult scenario for the production approach; the symmetry axes are nearly 45° from the acquisition axes, which makes the apparent moveout velocities along the x and y axes practically equal. A production velocity analysis is likely to not even detect the anisotropy in this case, because viewed from the acquisition axes, event B appears isotropic. The time-slice panel of Figure 2b reveals the poor performance of the isotropic NMO correction along other source-receiver azimuths of event B.

By measuring the local slopes of an input CMP gather as a volumetric attribute, the geometry of each traveltime surface is captured, even away from the x and y acquisition axes. Figures 3a and 3b show sections of the automatically measured inline and crossline slope volumes for the CMP from Figure 2a. The time-slice views clarify that the slopes are measured in the x and y directions throughout the volume, not just along the x and y zero-offset axes. Comparison of the slope volumes with Figure 2a also shows that there are clearly non-zero slopes in areas without data. No initial slope fields were used to get these measurements, but the results of the plane-wave destruction filter application were regularized with a smoothing constraint by using shaping regularization (Fomel, 2007). This constraint is enforced to help ensure that the moveout correction varies both spatially and temporally in a stable fashion. In Figure 3c, the velocity-independent elliptically anisotropic moveout correction is applied using these slopes, and all of the events are flattened well in both directions. The time-slice view of Figure 3c now shows the overall superior performance of the velocity-independent correction, but also reveals its limitations. As events become steep relative to the trace spacing, local slope measurements can be aliased. Towards the corners of the example gather, the slopes become too steep to be measured reliably, and in these areas, the automatic moveout correction performs poorly. In field data, crossline trace spacing is often much coarser than inline spacing, which may lead to similar aliasing problems. However, the effects of aliasing can often be mitigated with a few simple extra steps. By first applying a constant velocity isotropic NMO correction to the data before measuring slopes, the events will be flatter and less likely to have aliased slopes at far offsets. An inverse NMO correction using the constant velocity can then be applied to the measured slopes. The constant velocity can then be converted to p_x and p_y components and added to the slope measurements to obtain the unaliased slope fields of the input CMP gather.

Another perspective of the same test is shown in Figures 4a and 4b. The traces from the synthetic CMP gather have been binned into offset and azimuth coordinates to display the familiar sinusoidal signature of azimuthal traveltime variations. The various squared traveltime shifts (t_Δ values) applied by the automatic NMO correction were computed during implementation using equation 8, and then stored as a volumetric attribute. For each of the events, time-slices of this volume are shown in

Figures 5a-5d. The elliptical variation is clearly displayed for events A, B, and C, but the subtle variation for event D makes it difficult to detect the apparent anisotropy. Each time-slice from the same volume was re-indexed into a vector following the scheme described in the previous section, and then fed into a least-squares solver for equation 15 to yield $\mathbf{W}(t_0)$. The results of this inversion are displayed in Figures 6a-6b. At the times of the events, all three parameters have been extracted accurately. The shaping regularization used to create smooth slope fields also leads to similar smoothness in the $\mathbf{W}$ estimates. Because of the random noise in the synthetic data, slope measurements away from events are also random. The best-fit surface through these random slopes tends to be a flat plane, which is characterized on a CMP gather by zero slowness, causing the W_x and W_y estimates to tend toward zero between events. It is important to note that the values shown in Figures 6a-6d each rely on the accuracy of the NMO shifts computed at the corresponding value of t_0. Only the sparse times of this synthetic CMP gather with data have meaningful slope estimates and therefore meaningful $\mathbf{W}$ and α estimates.

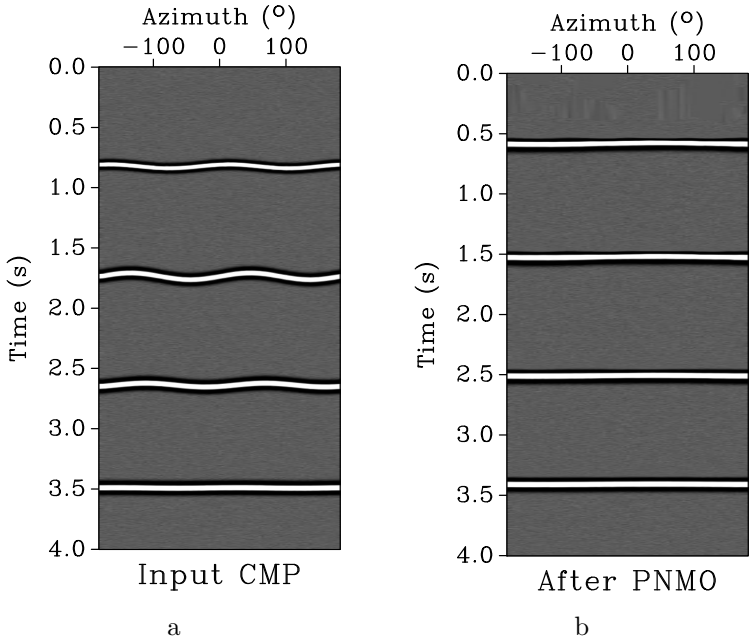

Figure 4: (a.) A common offset (0.75 km) display of CMP from Figure 2a with azimuth on the horizontal axis. (b.) The same traces after the automatic moveout correction. All events are shifted up to their appropriate t_0 and flattened.

The extracted moveout slowness matrices $\mathbf{W}(t_0)$ are used with equation 2 to estimate $\alpha(t_0)$. The results of estimating $\alpha(t_0)$ are displayed in Figure 6d, and the values at the times of each event are accurate. We conclude this example by solving for NMO slowness-squared as using $\alpha(t_0)$ and the corresponding eigenvalues at each t_0 with equation 5. These results, shown in Figures 7a-7d show that for all four events, the angle of anisotropy is detected. From this volume, the principal moveout directions are readily determined, the fast and slow axes are resolved, and the apparent anisotropy (the ratio or difference of V_{fast} and V_{slow}) is measurable.

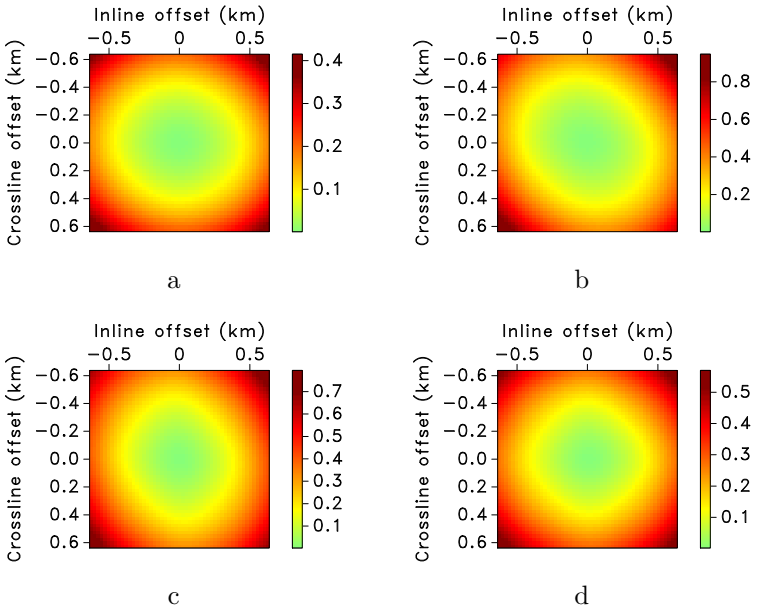

Figure 5: Traveltime squared shifts ($t_\Delta(t_0, x, y)$) for each event. (a.) Event A. (b.) Event B. (c.) Event C. (d.) Event D.

We next demonstrate a potential application of the automatic moveout correction on a real data example. In this case, we apply the automatic elliptically anisotropic moveout correction as a residual moveout correction. A subset of the McElroy data set from West Texas was formed into a supergather seen in Figure 8. Figure **??** shows a common offset (3.6-4.0 km) time-versus-azimuth display of the same data, where azimuthal anisotropy is evident for several events. In Figure **??**, the magnitude of the local slope is shown for the initial data. The areas with higher slope values highlight areas that were not ideally flattened by the prior isotropic NMO correction. The region of the highest slopes along the top of the figure is due to the proximity of the prior NMO mute at about 0.8 s. Figure **??** shows the results of applying two iterations of the proposed moveout correction. Further iterations will continue to flatten later events as distortions from overlying layers are removed. The events in the results are already noticeably flatter, and will therefore produce a cleaner stack.

DISCUSSION

Many advancements have been made in semi-automated traveltime picking schemes which have made the velocity analysis phase of a conventional seismic data processing flow much more efficient. However, a great deal of time is still required to manually check the quality of the assisted picking, and this remains as a time-consuming step in the conventional processing flow, especially in 3D. A similar procedure can be used for our velocity-independent approach. In production applications, the automatically measured slope fields from a subset of CMP gathers should be inspected manually.

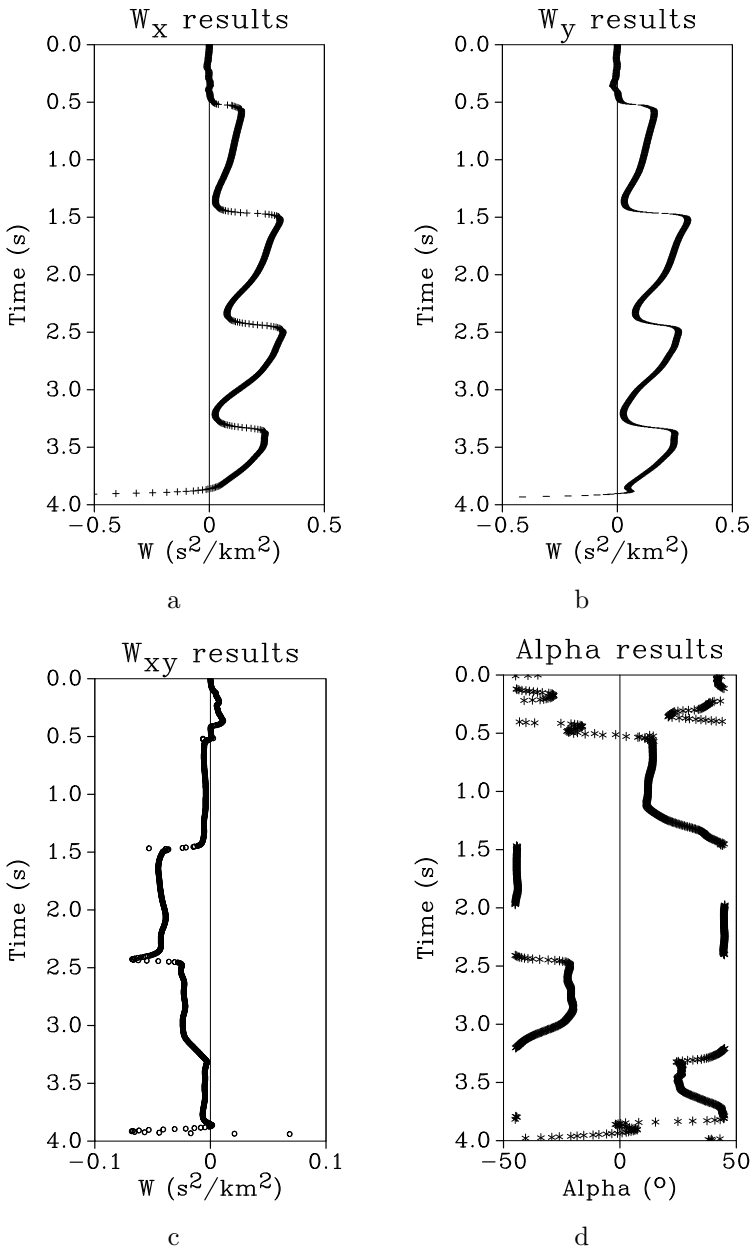

Figure 6: Elements of $\mathbf{W}(t_0)$ inverted from $t_\Delta(t_0, x, y)$ surfaces: (a.) W_x. (b.) W_y. (c.) W_{xy}. (d.) Azimuth angle $\alpha(t_0)$ computed from $\mathbf{W}(t_0)$.

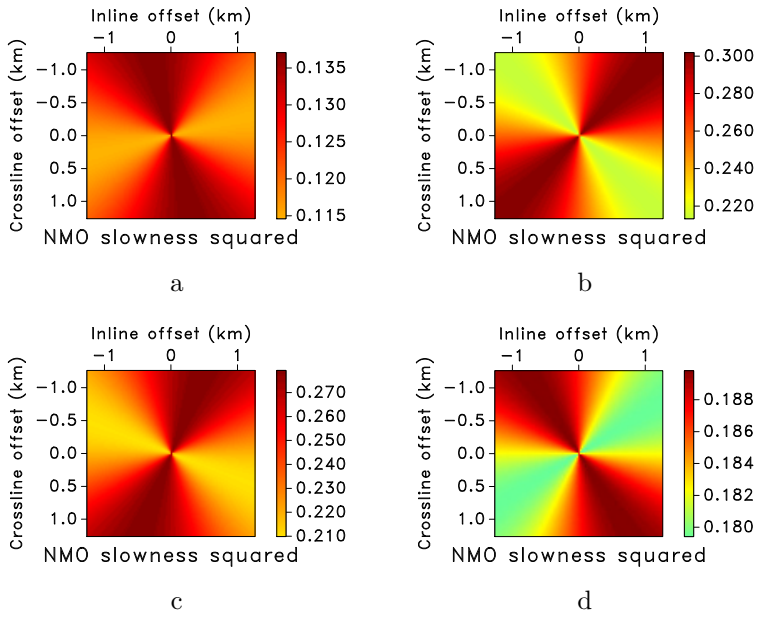

Figure 7: Time-slice views of NMO slowness-squared values computed for each event.(a.) Event A. (b.) Event B. (c.) Event C. (d.) Event D.

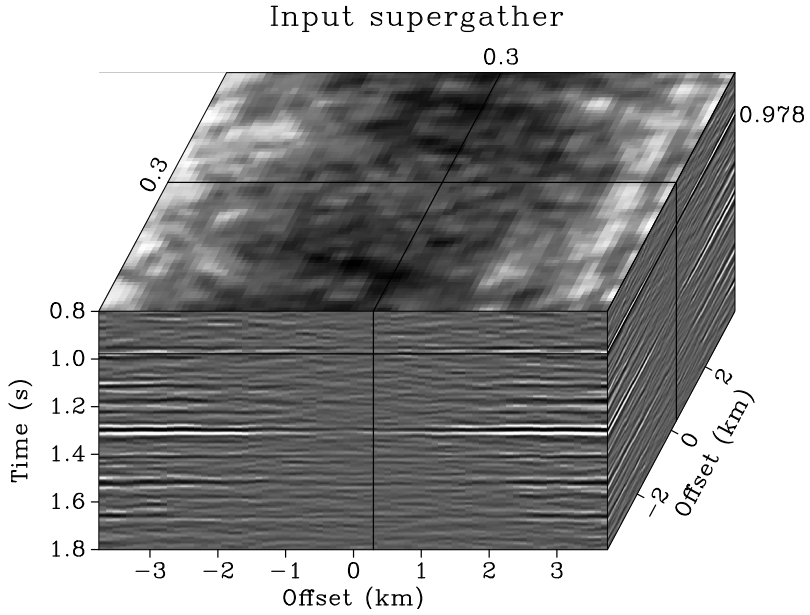

Figure 8: 3D view of a supergather from the McElroy data set, West Texas, US. Although the data has been isotropically NMO corrected, the time-slice view shows a subtle directional trend to the flatness of an event at 0.978 s.

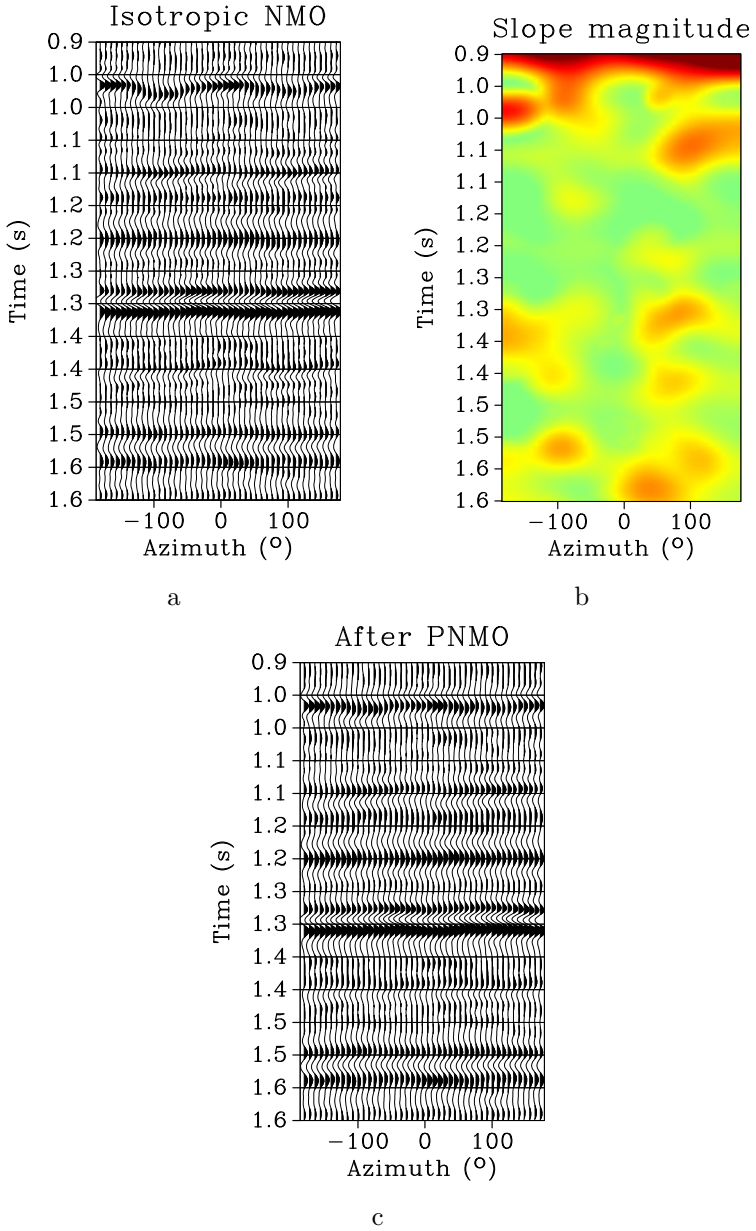

Figure 9: A time-versus-azimuth panel of traces for a range of offsets from 3.6-4.0 km from the McElroy data set. The central panel shows local slope magnitudes corresponding to the left input panel. The slope magnitude was computed as $\sqrt{p_x^2 + p_y^2}$. The same data after an automatic moveout correction has been applied as a residual moveout correction is shown on the right.

Slopes are very intuitive to understand and easy to compare to the input data. An overlay or side-by-side display of the two, combined with the NMO performance provide efficient and accurate quality control criteria.

Plane-wave destruction filters provide a truly automated approach to velocity analysis, as they can be used without any user-selected input parameters. Here, we have used the finite-difference plane-wave destructors, which, as described by Fomel (2002), can be given a user-supplied initial estimate of the slope field. Providing an initial slope estimate helps improve the efficiency of the slope-detection and can help estimate conflicting slopes (Fomel, 2002). In all of the examples above, no initial slope field was provided. The output slope fields are computed using smoothing regularization, which helps make the moveout correction more robust, and provides a way for the user to interact with the slope detection performance. If the seismic data is particularly noisy, a more aggressive smoothing can help make a more consistent automatic NMO correction, while for clean data, less smoothing yields a better resolved localized slope field.

We would like to comment here on the performance of the method for realistic cases containing a stack of layers, each with a different orientation of azimuthal anisotropy. The azimuthally-dependent traveltime variations caused by wave propagation in the upper layers will be superimposed on the reflection events corresponding to underlying layers. While inverting for NMO parameters is shown to be straightforward through the velocity-independent approach, solving for interval parameters would require these effects to be unraveled through the use of layer-stripping (Hake, 1986) or a Dix-type inversion (Grechka et al., 1999; Grechka and Tsvankin, 2002). If the effects from overlying layers distort later traveltime surfaces enough such that they are no longer elliptically hyperbolic as suggested by equation 1, then the moveout correction will not be complete for the entire section. However, as seen in the second example in the previous section, the velocity-independent moveout method can be used as a residual correction, with no changes to the procedure. The later events with incomplete moveout correction can therefore be corrected with iterated applications of the method. Another complication arises in the residual moveout case though, if one wants to extract parameters such as the azimuth angle or moveout slownesses. The equations presented here for parameter extraction were derived for a single pass NMO correction; it remains for further work to extend the parameter estimation methods to cases where residual moveout correction is necessary.

CONCLUSIONS

Measuring local slopes is a thorough and azimuthally flexible way to characterize traveltime surface geometry, which, in the 3D case, provides useful information about azimuthal variations in moveout velocity. We have demonstrated an application for this feature in performing an elliptically anisotropic moveout correction in 3D. No velocities are picked in order to perform this moveout correction, and since we use plane-wave destruction filters to measure local slopes, the entire process is automated.

Local moveout velocities can be calculated as a function of the local slopes, and the azimuthal angle of anisotropy can be estimated locally if one measures the first mixed-derivative of the traveltime surfaces at each point. By recording the traveltime shifts applied by our automated method, we formulate a highly overdetermined linear system to solve for moveout parameters as a function of time. This inversion scheme was shown to be very accurate on a synthetic data example, but remains to be tested on field data. The only practical limitation in the synthetic example comes from steeply dipping events which introduce aliased slope measurements. Although this type of aliasing can be mitigated to some extent with additional processing, further testing will be required on typical field geometries with relatively coarse crossline spacing.

Even in multi-layer cases, where conflicting azimuthal anisotropies are present, the proposed moveout correction itself can be performed accurately and automatically without velocity or parameter estimation. In these cases, the effective moveout parameters can be estimated from our method. Extensions of this method following an iterative scheme analogous to a layer-stripping or Dix-type inversion strategy may provide a powerful option to automatically recover interval parameters as well.

ACKNOWLEDGMENTS

We would like to thank Thomas Browaeys, Vladimir Bashkardin, Xiaolei Song, Paul Murray, and Jim Simmons for helpful discussions and suggestions. We would also like to thank Chevron for providing the McElroy data set.

This publication is authorized by the Director, Bureau of Economic Geology, The University of Texas at Austin.

REFERENCES

Crampin, S., 1984, Effective anisotropic elastic constants for wave propagation through cracked solids: Geophysical Journal of the Royal Astronomical Society, **76**, 135–145.

Fomel, S., 2002, Applications of plane-wave destruction filters: Geophysics, **67**, 1946–1960.

———, 2007, Velocity-independent time-domain seismic imaging using local event slopes: Geophysics, **72**, S139–S147.

Grechka, V., and I. Tsvankin, 1998, 3-D description of normal moveout in anisotropic inhomogeneous media: Geophysics, **63**, 1079–1092.

———, 2002, NMO-velocity surfaces and Dix-type formulas in anisotropic heterogeneous media: Geophysics, **67**, 939–951.

Grechka, V., I. Tsvankin, and J. K. Cohen, 1999, Generalized Dix equation and analytic treatment of normal-moveout velocity for anisotropic media: Geophysical Prospecting, **47**, 117–148.

Hake, H., 1986, Slant stacking and its significance for anisotropy: Geophysical Prospecting, **34**, 595–608.

Levin, F. K., 1985, Apparent velocity from dipping interface reflections: Geophysics, **50**, 2026–2032.

Lynn, W., 2007, Uncertainty implications in azimuthal velocity analysis: 77th Annual International Meeting, Society of Exploration Geophysicists, Expanded Abstracts, 84–88.

Ottolini, R., 1983, Velocity independent seismic imaging, *in* SEP-37: Stanford Exploration Project, 59–68.

Sicking, C., and S. Nelan, 2008, Azimuthal attribute methodologies: comparison of NMO super gathers, sectored isotropic migration, iterative azimuthal migration: 78th Annual International Meeting, Society of Exploration Geophysicists, Expanded Abstracts, 983–987.

Sicking, C., S. Nelan, and W. McLain, 2007, 3D azimuthal imaging: 77th Annual International Meeting, Society of Exploration Geophysicists, Expanded Abstracts, 2364–2367.

Siliqi, R., D. L. Meur, F. Gamar, L. Smith, J. Toure, and P. Herrmann, 2003, High-density moveout parameter fields V and Eta, Part 1: Simultaneous automatic picking: 73rd Annual International Meeting, Society of Exploration Geophysicists, Expanded Abstracts, 2088–2091.

Treadgold, G., C. Sicking, V. Sublette, and G. Hoover, 2008, Azimuthal processing for fracture prediction and image improvement: 78th Annual International Meeting, Society of Exploration Geophysicists, Expanded Abstracts, 988–992.

Weisstein, E. W., 2009, "Quadratic Curve" from MathWorld–A Wolfram Web Resource. (http://mathworld.wolfram.com/QuadraticCurve.html, accessed 14 April 2009).

Williams, M., and E. Jenner, 2002, Interpreting seismic data in the presence of azimuthal anisotropy; or azimuthal anisotropy in the presence of the seismic interpretation: The Leading Edge, **21**, 771–774.

Wolf, K., D. A. Rosales, A. Guitton, and J. Claerbout, 2004, Robust moveout without velocity picking: 74th Annual International Meeting, Society of Exploration Geophysicists, Expanded Abstracts, 2423–2426.